Effect of Augmented Collisional Ionization and potential depth in the VUV regime; a theoretical study

Nicolas Bigaouette* and Lora Ramunno†
Department of Physics, University of Ottawa, 150 Louis Pasteur, Ottawa ON, K1N 6N5, Canada

Edward Ackad‡
Department of Physics, Southern Illinois University Edwardsville, State Route 157 Edwardsville, IL 62026, United States

(Dated: August 26, 2013)

We revisit the 2002 experiment at FLASH-DESY FEL facilities on Xenon clusters interacting with VUV (98 nm, 12.65 eV) 100 fs laser pulses, in light of a re-calibration of the intensity to 40% of its originally quoted value. We found that augmented collisional ionization, a mechanism we recently investigated for XUV-cluster interactions, increases the maximum charge state by two, and gives a maximum charge state and most abundant charge state compatible with experimental observations. Further, we found a significant effect of potential depth, which further increases agreement with experiment.

I. INTRODUCTION

The advance of Free Electrons Lasers (FEL) around the world gave access to unprecedented intensity at wide range of wavelengths, including from the VUV to X-ray. Recent experiments have studied the interaction of such laser pulses with clusters of atoms. These clusters are nanoscopic objects at solid density. Additionally, their finite size makes them easier to study, both theoretically and experimentally.

Many studies of the interaction of laser-matter have been done at wavelengths ranging from the IR to X-ray regimes. Experiments in 2002 by Wabnitz *et al.*[1] at FLASH-DESY FEL facilities on clusters of Xenon and VUV radiation saw surprisingly high charge states (Xe^{8+}) using 98 nm (12.7 eV). The heating and ionization mechanisms known at that time could not explain the high charge states; more work was required. Three major models emerged to explain these high ionization levels.

First, the lowering of the potential barrier was suggested for photo-ionization [3–6] where a neighbouring ion lowers the barrier, making the absorption of a single photon by the electron energetically possible.

Second, Santra and Green suggested using atomic potential instead of the Coulomb potential. They used a simple screening potential [7] and later a more realistic one [8] based on a Hartree-Fock-Slater code written by F. Herman and S. Skillman [9] and saw 30 times more VUV photons absorbed by a cluster environment compared with using a Coulomb potential. Charge states up to Xe^{6+} for Xe_{1500} clusters were obtained with simulations using the atomic potentials.

Jungreuthmayer *et al.*[2] identified an additional mechanism dubbed "Multi-Body Recombination" (MBR) heating. Through laser-cluster simulations based on classical dynamics, they showed that the created plasma is cold and dense enough to fall within the strongly coupled plasma regime. As such, the plasma is highly collisional and via multiple collisions electrons can recombine to a highly excited state with high probability. This newly recombined electron can then reabsorb a new photon from the laser, effectively increasing the system's energy absorption from the laser.

In 2010, the intensity of the DESY-FEL pulses[1] was re-calibrated to be 40% of the originally quoted value [10]. The question now arises: given that the previous models showed good agreement with experimental result at the originally quoted intensity, is there something potentially missing from the previous models in light of this intensity adjustment? In this paper, we investigate two possible effects that might contribute.

First, our group recently investigated the involvement of atomic excited states in collisional ionization in laser-cluster interaction experiments in the XUV[11–13]. We presented a model wherein collisional ionization is allowed to occur in two steps. First, a colliding electron may promote a bound electron to an excited state. Then another colliding electron may promote this excited one into the conduction band. This allows lower-energy electrons to ionize an atom/ion, where such ionization would not be possible via the usual single-step collisional ionization models. We called this process "Augmented Collisional Ionization" (ACI), and we now seek to investigate its role in the VUV laser-cluster regime. We do this via a classical model similar to that employed by Jungreuthmayer *et al.*

Second, we investigate the effect of the electron-ion potential in classical simulations, given the large effect of potential shape on VUV-cluster interaction found by Santra and Green. Though in this work we only use the Coulomb potential, we investigate how the potential

depth of the softened version affects simulation outcomes. This provides some hints as to how a different potential shape may interact with classical simulations.

In the first part of this paper, we will describe our classical approach to the clusters' dynamics followed by the different ionization processes which are treated quantum mechanically. Results are then presented by first showing the influence ACI has on the maximum charge states seen in simulations. Then, the cluster size influence is studied and compared to experiments by averaging over the spatial distribution of the laser pulse. Last, we investigate the influence of the potential depth used in our simulations on the maximum charge state seen.

II. MODEL

Clusters are nanoscopic systems and as such are hard to model using statistical approaches which often assume infinite systems. Our model thus tracks every particle present using a classical molecular dynamics (MD) code. Such MD codes are excellent tools for the simulation of a low number of particles since no approximation is used (apart from the classical instantaneous electrostatic interactions). Unfortunately, the N-body problem has no analytic solutions and is chaotic, requiring large amount of data for valid statistics. Furthermore, the MD interaction calculation has an $O(N^2)$ scaling which renders simulations of tens of thousands of particles using long range interactions virtually impossible. Approximations to the N-body problem are possible; hierarchical tree code [14] and fast-multipole methods [15] can reduce the burden to an $O(N \log(N))$ problem.

These algorithms have overheads which makes them slower for a lower number of particles. They can also introduce some errors in the force and potential calculations. While these errors are not significant for the dynamics aspect of the simulation, they can influence the calculated rates of quantum transitions. We instead decided to port the classical dynamics aspect of the simulation to the OpenCL framework. This allows us to accelerate calculation on general-purpose graphical processing units (GP-GPU), bringing a speed up of between 40 and 80 times.

The Coulomb interaction between particles is softened at small distances to avoid numerical errors due to the singularity. Particles are treated as Gaussian charge densities where the potential is given by (in atomic units):

$$\phi(r) = \frac{Z}{r}\mathrm{erf}\left\{\frac{r}{\sigma\sqrt{2}}\right\} \tag{1}$$

with erf the error function, Z the charge state of the particle and σ the width of the charge density given by:

$$\sigma = \frac{Z}{D}\sqrt{\frac{2}{\pi}} \tag{2}$$

The maximum depth of the potential of a $Z = 1$ ion is given by the parameter D. At large distances ($r >> \sigma$), this smoothed potential converges to the Coulomb potential.

Initially, the simulated cluster is a collection of neutral atoms. As time passes, the laser is modelled as both an oscillating electric field with a carrier envelope and a flux of photons. Electrons and ions are created in the code by ionization events modelled via quantum rates. These are now described in the following section.

A. Single photon ionization

The first step in the interaction is single photon ionization of the neutral atoms. As such ionization events occur, the laser amplitude is depleted. Experimental cross sections for Xenon in the VUV regime were taken from experimental data [16]. These cross-sections are converted to rates and a Monte-Carlo test evaluates the ionization probability.

At the studied intensities (10^{12} to 10^{13} W/cm^2) and wavelength (98 nm, 12.65 eV), tunnel ionization is negligible, as is multi-photon absorption. In addition, ions cannot be further ionized via single photon ionization.

B. Threshold V_p

Many processes are modelled using quantum rates known for isolated atoms. For example, the semi-empirical Lotz cross-sections for impact ionization assumes the impacting electron comes from infinity where its potential energy is null. However the cluster environment must be taken into account. We model these interactions as those of an isolated system residing in a constant potential created by the cluster environment. This potential V_p is the contribution of all particles outside the nearest neighbour distance in the pre-ionized cluster.

C. Impact ionization

Impact ionization is implemented using the semi-empirical Lotz cross-sections[17] with parameters taken from references [18] for the neutral and [19] for ionized Xenon. The impact parameter b of the impacting electron is calculated through $b = |\mathbf{v} \times \mathbf{r}| / |\mathbf{v}|$ where $\mathbf{v}$ is the impacting electron's velocity vector and $\mathbf{r}$ the vector from the impacting electron to the target. If the impact parameter lies inside the calculated cross section, ionization takes place. We take the impacting electron's total energy with respect to the threshold V_b as its effective kinetic energy.

D. Augmented Collisional Ionization (ACI)

In recent work, we introduced a model [12] which we dubbed "Augmented Collisional Ionization" (ACI) that

we applied to Argon experiments at 32.8 nm [20] and Xenon clusters in soft X-rays (13.7 nm, 90.5 eV)[13, 21]. We now port that model over to the VUV regime.

In the ACI model, electrons are created in a two step process. After an electron collides with an atom or ion, we allow for the final state to be an excited atom or ion plus a reduced-energy impact electron. Once excited, an atom or ion can be impact-ionized more easily by a second, lower energy, impacting electron. ACI thus allows electrons in the lower energy tail of the kinetic energy spectrum to contribute to the cluster ionization. Additionally, more ionization paths are present in the model.

ACI is modelled similarly to impact ionization. Cross sections for the different transitions are taken from a Hartree-Fock implementation of the Cowan code[22]. For this work on Xenon clusters, eight excited states ($l < 4$) per charge state are used, for ionization levels up to Xe^{17+}.

E. Ground state recombination

We include in our model recombination to the ground state as described in detail in our previous work [13]. If an electron's total energy with respect to the V_p threshold becomes lower than the ground state energy, this electron is recombined with the parent ion and disappears from the simulation. The ion's charge state is updated to reflect the process.

This allows having a potential that is as close as Coulombic as possible (except at really close range where the potential converges to $\phi = ZD$) without having electrons with classical energy below the ground state. Interestingly, it also accelerates the $O(N^2)$ force calculation by reducing the number of particles in the system.

F. Many Body Recombination

MBR is automatically included in a classical MD simulation and is thus included in our results.

An important distinction between MBR and ACI is the direction in which the electronic transition takes place. In the case of ACI, the transition is going "up the energy ladder": a bound electron first in the ground state will receive energy from an impacting electron. Afterwards, the excited atom is ionized more easily by other impacting electrons due to, firstly, the cross-section of the excited state to continuum state being larger than the cross-section from the ground state to continuum. Secondly, the energy required for the excited state to continuum transition is less than that of the ground state to continuum transition and as such more free electrons have a chance to ionize the excited atom. On the other hand, MBR is a transition from the continuum to a highly excited state. While the later is treated purely classically, the former is implemented using cross-sections taken from a Hartree-Fock calculation. The lower excited states used in ACI are distant from each other and must be treated discretely while the higher states in MBR are so dense that their classical treatment does not result in much error.

III. RESULTS

A. Effect of Augmented Collisional Ionization

We examine the effect of ACI by performing VUV-cluster interaction simulations for a range of VUV intensities, and a range of cluster sizes, both with and without the ACI mechanism enabled in our code. The small nature of these clusters, the random process of the Monte-Carlo ionization procedures and the chaotic nature of the many-body problem requires acquiring a large sample for valid statistics; 5,000 simulations were run for small clusters, and 100 for larger clusters. The Coulomb potential depth is limited at close range to prevent the large field close to the discontinuity from cause numerical heating. In this subsection, equation (1) is used with $D = 12$ eV. Cross-sections were taken from experimental data from reference [16] for single photon ionization. For impact ionization, experimental cross-sections from references [18] and [19] rather than Lotz [17] were used.

When irradiated with a 98 nm (12.95 eV) laser pulse, all atoms in the cluster become rapidly ionized to $Z = +1$. This is due to the fact that single photon ionization cross-section is largest (68 Mb) at this longer wavelength for neutral Xenon. Since the photon energy is not sufficient to ionize an isolated Xe^{1+} to Xe^{2+}, only the first charge state is accessible through single photon ionization in our model. Larger charge states are caused by other mechanisms as is evidenced by experiments with gas targets.

The cluster dynamics after the laser pulse is mainly an expansion; no significant ionization has been observed during that time. As such, simulations were run up to 400 fs which is approximately 150 fs after the end of the laser pulse. We have not seen any major changes when continuing the simulations for longer times.

We first compare the highest charge states seen in both our simulations and the 2002 experiment at DESY with the re-calibrated intensity values [10]. We do this by running simulations close to experimental parameters at the peak laser intensity only.

We ran simulations with Xe_{90} clusters to compare with Figure 1 of Wabnitz *et al.* at the revised intensity of 8×10^{12} W/cm^2. Figure 1 shows the resulting charge state spectrum. The left subplot shows data when ACI is not enabled, while the right subplot shows the spectrum when ACI is enabled, with the ratio of excited states in hatched regions. As we can see, ACI increases by two the maximum charge state from Xe^{3+} to Xe^{5+}. The 2002 experiment showed a clear signal for at least Xe^{4+} for Xe_{80} clusters. Without ACI, there is only a very small, almost negligible, fraction of Xe^{3+} while there is signifi-

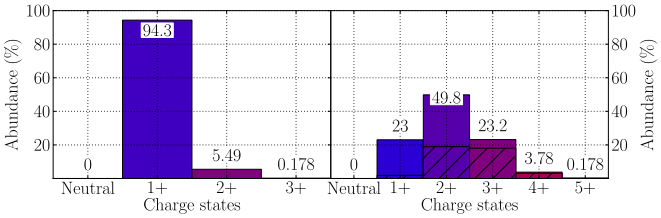

FIG. 1: Charge states spectra of Xe_{90} clusters at $8{\times}10^{12}$ W/cm^2 with ACI disabled (left) and enabled (right)

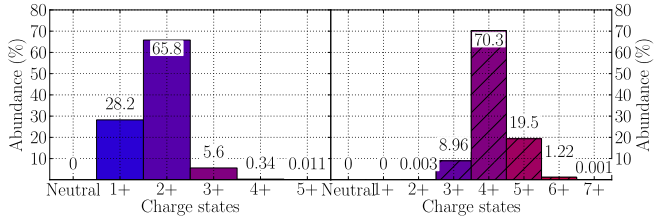

FIG. 2: Charge states spectra of Xe_{1000} clusters at $1.5{\times}10^{13}$ W/cm^2 with ACI disabled (left) and enabled (right)

cant abundance of Xe^{4+} when ACI is enabled; this corresponds more closely to the highest charge state seen in the experimental data. Further, we see by the hatched areas on the right graph, that at the end of the simulation with ACI enabled, there are a large percentage of ions that are in an excited state, that is, that have gone through one step of the two step ACI process.

We also ran simulations of $Xe_{1,000}$ clusters at 1.5×10^{13} W/cm^2, which is close to the experimental parameters of the largest intensity plot of Figure 1 of Wabnitz *et al.*, assuming a similar recalibration. We plot the charge spectra with and without ACI in Figure 2. When ACI is disabled, the maximum (significant) charge state seen is Xe^{4+}, whereas the maximum (significant) charge state of Xe^{6+} if found when ACI is enabled. We note however that our simulated intensity value is somewhat lower than the expected re-calibrated experimental value, so this is a lower bound. Nevertheless, this is an indication that ACI may play a vital role in the dynamics.

To compare to the previous theoretical work of Jungreuthmayer *et al.* [2], we also measured the number of electrons which are in a many-body recombined (MBR) state. We found that around 18 % of the total number of electrons are in an MBR state starting from around the peak of the laser pulse through the end of the simulations, close to the previous value found of around 25 %. This is an indication that MBR is still important in the description of the dynamics.

The previous results can only predict the highest charge state seen because only the intensity at the peak was considered in our simulations. As such, the charge state distributions we observed in figures 1 and 2 have a much higher most abundant charge state than seen in experiment. Thus, we next consider the effect of the spatial profile of the laser pulse.

Distance to focus	Normalized height	Intensity ($\times 10^{12}$ W/cm^2)
0	1	8.000
$\sqrt{-2\sigma^2 \ln\left(\frac{1+e^{-1/2}}{2}\right)}$	$\frac{1+e^{-1/2}}{2}$	6.424
σ	$e^{-1/2}$	4.852
$\sigma\sqrt{2\ln(2)}$	1/2	4.000
$\sqrt{2}\sigma$	e^{-1}	2.943
2σ	e^{-2}	1.083

TABLE I: Intensity of laser pulse at different distances of the focus assuming a gaussian spatial profile with a standard deviation σ.

We take the density of clusters coming out of the nozzle to be constant in space over the laser focal volume. As such, the clusters distributed across focal volume will sample a different laser intensity depending on their location. For a given peak intensity value and cluster size, we then run a series of simulations at different intensities. The resulting spectra are then weighted accordingly.

We perform simulations with spatial averaging for the re-calibrated peak intensity 8×10^{12} W/cm^2, corresponding to Figure 1 of Wabnitz *et al.*. Similarly to that figure, we also study the effect of cluster size. However, due to computational resources limits, the largest clusters we simulated were $Xe_{5,083}$, whereas in the experiment it was $Xe_{30,000}$ (revised in 2010 to $Xe_{90,000}$). Our spatial averaging was done with weight values presented in Table I. Considering a focus diameter (FWHM) of $\tau = 20\mu$m we have $\sigma = \tau\left(2\sqrt{2\ln(2)}\right)^{-1} = 11.77\mu$m.

For this set of simulations, we forcibly recombine, at the end of every simulation, electrons that are closer than 4 Bohr to an ion and have a negative energy. This energy is calculated as the electron's kinetic energy plus the potential energy between this electron and the nearby ion. This is the most conservative estimate of what would be detected in an actual experiment

Figure 3a shows the charge state distribution for Xe_{90} clusters and figures 3b, 3c and 3d show the distribution of icosahedral clusters with their 7^{th}, 8^{th} and 11^{th} closed shells ($Xe_{1,415}$, $Xe_{2,057}$ and $Xe_{5,083}$, respectively). All icosahedral configurations were relaxed using a Lennard-Jones potential for neutral xenon.

For each cluster size, we see spatial averaging gives most abundant charge states that are more in-line with experimental observations, as expected. Enabling ACI increases the highest charge states (with significant abundance) in each case by one or two, with the largest change seen for the largest cluster size. Additionally, the most abundant charge state is shifted from Xe^{1+} to Xe^{2+} when ACI is enabled for large clusters, while staying at Xe^{1+} for the smallest (Xe_{90}) clusters. Similar to experiment, we see the general trend that the highest charge states

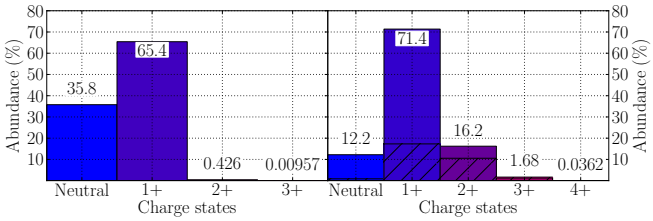

(a) Xe_{90}

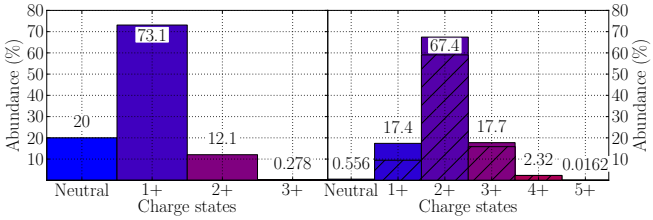

(b) $Xe_{1,415}$

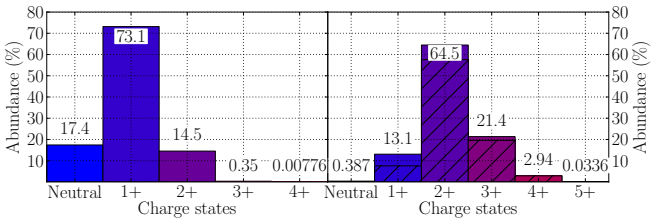

(c) $Xe_{2,057}$

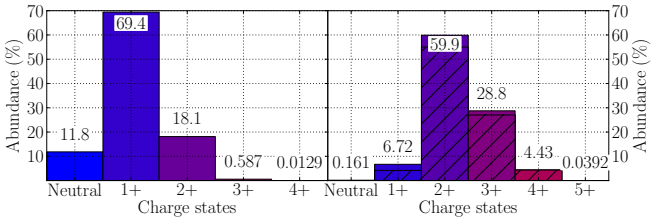

(d) $Xe_{5,083}$

FIG. 3: Charge states spectra of different cluster sizes using intensities of table I. ACI disabled (left) and enabled (right)

and the distributions in general are shifting to larger values as the cluster size increases.

It is interesting to note that the Xe^{3+} population doubles between the $Xe_{1,415}$ and $Xe_{5,083}$ clusters. Though $Xe_{5,083}$ clusters are less than four times larger than $Xe_{1,415}$, they have 4 more closed shells. The doubling of the Xe^{3+} is likely caused by the number of ions on the cluster surface increasing more slowly than the number of ions in the cluster volume. For example, the $Xe_{1,415}$ clusters have 35 % of atoms inside their volume, while this proportion drops to 24 % for $Xe_{5,083}$. Since we have seen that the higher charge states reside on the cluster boundaries in XUV-cluster interaction, as reported in [11], we expect to see a slower increase of the yield of the highest charge states compared to the cluster size increase.

B. Effect of potential depth

In previous studies[7, 8] the shape and depth of the ion potential was found to have a large influence through increased inverse Bremsstrahlung heating (IBH). The potential depth parameter of 12 eV used above prevents electrons from falling too deep within an ion's potential well. Using deeper potentials would allow the possibility for larger angle scattering and possibly increased IBH, even within the Coulomb potential used in this paper. To explore this avenue, however, we need to prevent electrons from acquiring too low an energy. We do this by employing ground state recombination model developed in our previous work[13]. This allows us to use a deeper potential while preventing numerical heating.

As the potential gets deeper, the field close to the ion increases and a smaller time step must be used for simulations, significantly increasing the computational resources required. We used a very small time step of 0.15 as which minimizes the calculation error while still providing reasonable simulation duration. We compared the results that follow with simulations run with a smaller time step of 0.1 as and found only negligible differences in the charge states distribution. Additionally, since recombination will change the charge state distribution even after the laser has passed by redistributing energy throughout the cluster, simulations must be run for a longer time. In this case, simulations went up to 1 ps where the cluster is fully exploded. Because of this increase computational load, we did not perform spatial averaging for the results that follow. Also, due to the smaller time step used in this section not as many runs could be performed as was done in the previous section; 60 runs were used to generate every charge state spectrum shown on figures 4

We find that the depth of the potential does have an influence on the cluster dynamics. Figures 4a and 4b show the results for Xe_{80} clusters under a 8×10^{12} W/cm^2 laser pulse for a potential depth parameter D of 27.2 eV (1 Eh) and 81.63 eV (3 Eh) – see equation (2). Refer to figure 1 for the corresponding simulation done at D =12 eV (0.441 Eh).

We clearly see an increase in both the maximum and dominant charge state seen as the potential depth parameter increases. While the shallow potential depth of 12 eV gives interesting results, we see that a deeper potential is required to obtain higher charge states, most notably, a sizable Xe^{4+} population. This is relevant because when forcible recombination was applied to the comparable Xe_{90} simulations with spatial averaging (see Figure 3a), there was not a significant Xe^{4+} population that remained.

We see that for D = 3 Eh, the distribution is similar to that with D = 1 Eh. This is very interesting, and indicates the saturation of the energy absorption. This suggests that large-angle scattering also saturates.

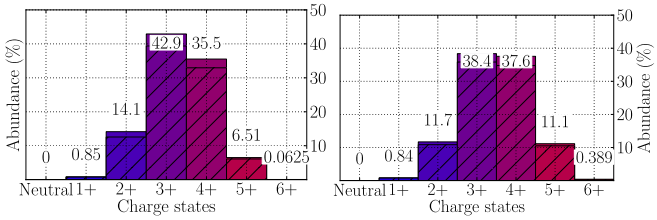

(a) $D = 27.2$ eV (1 Eh) (b) $D = 81.63$ eV (3 Eh)

FIG. 4: Charge state spectra after 1 ps of Xe_{80} using an intensity of 8×10^{12} W/cm^2 and different potential depths D (see equation (2)). ACI is enabled for both figures.

IV. CONCLUSION

We revisited the 2002 VUV-Xenon cluster experiment at DESY, in light of the recent recalibration of the VUV laser intensity to a much lower value. We applied a classical dynamics model to study the influence of augmented collisional ionization and potential depth and found that ACI does influence both the maximum charge state and distributions. For Xe_{80} clusters at 8×10^{12} W/cm^2 and Xe_{1000} clusters at 1.5×10^{13} W/cm^2, the maximum charge state seen was increased by two when ACI was enabled, giving results that are more compatible with the 2002 DESY experiment than when ACI was not included. This give an indication that ACI may plays an important role in the cluster dynamics. We also performed spatial averaging over the laser pulse, and found a most-abundant charge state that was compatible with experiment when ACI was enabled, for a range of cluster sizes. Finally, we looked at the potential depth influence on charge state spectra. We applied a model that allows recombination to the ground state to prevent artificial electrons heating. We found that using a deeper potential in our classical code does result in higher charge states, though the effect of this saturates at a depth of around 1 Hartree. Implementing a more realistic atomic potential rather than a Coulomb potential would be an interesting further extension of this work.

[1] H. Wabnitz, L. Bittner, A. R. B. de Castro, R. Dhrmann, P. Grtler, T. Laarmann, W. Laasch, J. Schulz, A. Swiderski, K. von Haeften, T. Mller, B. Faatz, A. Fateev, J. Feldhaus, C. Gerth, U. Hahn, E. Saldin, E. Schneidmiller, K. Sytchev, K. Tiedtke, R. Treusch, and M. Yurkov, Nature **420**, 4825 (2002).

[2] C. Jungreuthmayer, L. Ramunno, J. Zanghellini, and T. Brabec, Journal of Physics B: Atomic, Molecular and Optical Physics **38**, 30293036 (2005).

[3] C. Siedschlag and J.-M. Rost, Physical Review Letters **93**, 43402 (2004).

[4] U. Saalmann and J.-M. Rost, Physical Review Letters **91** (2003), 10.1103/PhysRevLett.91.223401.

[5] U. Saalmann, C. Siedschlag, and J.-M. Rost, Journal of Physics B: Atomic, Molecular and Optical Physics **39**, R39R77 (2006).

[6] I. Georgescu, U. Saalmann, and J.-M. Rost, Physical Review A **76**, 18 (2007).

[7] C. Greene and R. Santra, Physical Review Letters **91**, 14 (2003).

[8] R. Santra and C. Greene, Physical Review A **70** (2004), 10.1103/PhysRevA.70.053401.

[9] F. Herman and S. Skillman, *LANL* (Prentice-Hall, 1963).

[10] C. Bostedt, M. Adolph, E. Eremina, M. Hoener, D. Rupp, S. Schorb, H. Thomas, A. R. B. de Castro, and T. Mller, Journal of Physics B: Atomic, Molecular and Optical Physics **43**, 194011 (2010).

[11] E. Ackad, N. Bigaouette, K. Briggs, and L. Ramunno, Physical Review A **83**, 063201 (2011).

[12] E. Ackad, N. Bigaouette, and L. Ramunno, Journal of Physics B: Atomic, Molecular and Optical Physics **44**, 165102 (2011), arXiv:1011.5216.

[13] E. Ackad, N. Bigaouette, S. Mack, K. Popov, and L. Ramunno, New Journal of Physics **15**, 053047 (2013).

[14] J. E. Barnes and P. Hut, Nature **324**, 446449 (1986).

[15] P. Gibbon and G. Sutmann, in *Quantum Simulations of Complex Many-Body Systems: From Theory to Algorithms*, NIC Series, Vol. 10 (2002) p. 467506.

[16] J. B. West and J. Morton, Atomic Data and Nuclear Data Tables **22**, 103107 (1978).

[17] W. Lotz, Zeitschrift fur Physik **206**, 205211 (1967).

[18] H. Tawara and T. Kato, Atomic Data and Nuclear Data Tables **36**, 167353 (1987).

[19] A. Heidenreich, I. Last, and J. Jortner, The European Physical Journal D **35**, 567577 (2005).

[20] C. Bostedt, H. Thomas, M. Hoener, E. Eremina, T. Fennel, K.-H. Meiwes-Broer, H. Wabnitz, M. Kuhlmann, E. Plonjes, K. Tiedtke, R. Treusch, J. Feldhaus, A. R. B. de Castro, and T. Moller, Physical Review Letters **100**, 133401 (2008).

[21] H. Thomas, C. Bostedt, M. Hoener, E. Eremina, H. Wabnitz, T. Laarmann, E. Plnjes, R. Treusch, A. R. B. de Castro, and T. Mller, Journal of Physics B: Atomic, Molecular and Optical Physics **42**, 134018 (2009).

[22] R. D. Cowan, *Nature*, Los Alamos Series in Basic and Applied Sciences, Vol. 140 (University of California Press, 1981) Chap. 8 and 16, p. 626627.

[23] M. Y. Amusia, *Atomic Photoeffect* (Springer, 1990).

[24] J. E. Barnes, Journal of Computational Physics **87** (1990), 10.1016/0021-9991(90)90232-P.

[25] C. Bostedt, H. Thomas, M. Hoener, T. Mller, U. Saalmann, I. Georgescu, C. Gnodtke, and J.-M. Rost, New Journal of Physics **12** (2010), 10.1088/1367-2630/12/8/083004.

[26] T. Fennel, K.-H. Meiwes-Broer, J. Tiggesbumker, P. M. Dinh, and E. Suraud, Reviews of Modern Physics **82**, 17931842 (2010).

[27] M. Hoener, C. Bostedt, H. Thomas, L. Landt, E. Eremina, H. Wabnitz, T. Laarmann, R. Treusch, A. R. B. de Castro, and T. Mller, Journal of Physics B: Atomic, Molecular and Optical Physics **41**, 181001 (2008).

[28] B. Iwan, J. Andreasson, M. Bergh, S. Schorb, H. Thomas, D. Rupp, T. Gorkhover, M. Adolph, T. Mller, C. Bostedt, J. Hajdu, and N. Tmneanu, Physical Review A **86** (2012), 10.1103/PhysRevA.86.033201.

[29] H. Iwayama, A. Sugishima, K. Nagaya, M. Yao, H. Fukuzawa, K. Motomura, X.-J. Liu, A. Yamada, C. Wang, K. Ueda, N. Saito, M. Nagasono, K. Tono, M. Yabashi, T. Ishikawa, H. Ohashi, H. Kimura, and T. Togashi, Journal of Physics B: Atomic, Molecular and Optical Physics **43**, 161001 (2010).

[30] M. Krikunova, M. Adolph, T. Gorkhover, D. Rupp, S. Schorb, C. Bostedt, S. Roling, B. Siemer, R. Mitzner, H. Zacharias, and T. Mller, Journal of Physics B: Atomic, Molecular and Optical Physics **45**, 105101 (2012).

[31] T. Laarmann, A. de Castro, P. Grtler, W. Laasch, J. Schulz, H. Wabnitz, and T. Mller, Physical Review Letters **92** (2004), 10.1103/PhysRevLett.92.143401.

[32] T. Laarmann, M. Rusek, H. Wabnitz, J. Schulz, A. de Castro, P. Grtler, W. Laasch, and T. Mller, Physical Review Letters **95** (2005), 10.1103/PhysRevLett.95.063402.

[33] R. Moshammer, Y. Jiang, L. Foucar, A. Rudenko, T. Ergler, C. Schrter, S. Ldemann, K. Zrost, D. Fischer, J. Titze, T. Jahnke, M. Schffler, T. Weber, R. Drner, T. Zouros, A. Dorn, T. Ferger, K. Khnel, S. Dsterer, R. Treusch, P. Radcliffe, E. Plnjes, and J. Ullrich, Physical Review Letters **98** (2007), 10.1103/PhysRevLett.98.203001.

[34] D. Rupp, M. Adolph, T. Gorkhover, S. Schorb, D. Wolter, R. Hartmann, N. Kimmel, C. Reich, T. Feigl, A. R. B. de Castro, R. Treusch, L. Strder, T. Mller, and C. Bostedt, New Journal of Physics **14**, 055016 (2012).

[35] U. Saalmann, Journal of Physics B: Atomic, Molecular and Optical Physics **43**, 194012 (2010).

[36] M. Schffler, K. Kreidi, D. Akoury, T. Jahnke, A. Staudte, N. Neumann, J. Titze, L. Schmidt, A. Czasch, O. Jagutzki, R. Costa Fraga, R. Grisenti, M. Smolarski, P. Ranitovic, C. Cocke, T. Osipov, H. Adaniya, S. Lee, J. Thompson, M. Prior, A. Belkacem, T. Weber, A. Landers, H. Schmidt-Bcking, and R. Drner, Physical Review A **78**, 013414 (2008).

[37] Z. B. Walters, R. Santra, and C. H. Greene, Physical Review A **74**, 43204 (2006), arXiv:0510187v3 [arXiv:physics].

[38] B. Ziaja, H. Wabnitz, F. Wang, E. Weckert, and T. Mller, Physical Review Letters **102** (2009), 10.1103/PhysRevLett.102.205002.

[39] B. Ziaja, H. Wabnitz, E. Weckert, and T. Mller, New Journal of Physics **10**, 043003 (2008).

[40] J. Zweiback, T. Ditmire, and M. Perry, Physical Review A **59**, R3166R3169 (1999).

[41] M. Arbeiter and T. Fennel, New Journal of Physics **13**, 053022 (2011).

[42] D. Bauer, Journal of Physics B: Atomic, Molecular and Optical Physics **37**, 30853101 (2004).

[43] C. Deiss, N. Rohringer, J. Burgdrfer, E. Lamour, C. Prigent, J.-P. Rozet, and D. Vernhet, Physical Review Letters **96** (2006), 10.1103/PhysRevLett.96.013203.

[44] F. Dorchies, T. Caillaud, F. Blasco, C. Bont, H. Jouin, S. Micheau, B. Pons, and J. Stevefelt, Physical Review E **71** (2005), 10.1103/PhysRevE.71.066410.

[45] R. von Pietrowski, K. von Haeften, T. Laarmann, T. Mller, L. Museur, and A. V. Kanaev, The European Physical Journal D **38**, 323336 (2006).

[46] A. Kramida, Y. Ralchenko, J. Reader, and N. A. Team, "NIST Atomic Spectra Database (ver. 5.0)," (2012).